CHARACTERIZATION OF UV-LIGHT-DRIVEN Ag/BiOCl NANOPLATES SYNTHESIZED BY SONOCHEMICAL DEPOSITION METHOD

A. PHURUANGRAT[a*], P. DUMRONGROJTHANATH[b],
B. KUNTALUE[c], S. THONGTEM[d,e], T. THONGTEM[e,f]

[a] *Department of Materials Science and Technology, Faculty of Science,*
Prince of Songkla University, Hat Yai, Songkhla 90112, Thailand
[b] *Rajamangala University of Technology Lanna Chiang Rai,*
Chiang Rai 57120, Thailand
[c] *Electron Microscopy Research and Service Center, Faculty of Science,*
Chiang Mai University, Chiang Mai 50200, Thailand
[d] *Department of Physics and Materials Science, Faculty of Science,*
Chiang Mai University, Chiang Mai 50200, Thailand
[e] *Materials Science Research Center, Faculty of Science, Chiang Mai University,*
Chiang Mai 50200, Thailand
[f] *Department of Chemistry, Faculty of Science, Chiang Mai University,*
Chiang Mai 50200, Thailand

In this study, a facile strategy for the fabrication of Ag/BiOCl nanoplates for photodegradation of methylene blue (MB) under UV light irradiation is reported. BiOCl nanoplates were synthesized by simple hydrothermal method. Ag nanoparticles were deposited on BiOCl nanoplates in ethylene glycol as a solvent by sonochemical method. The as-prepared samples were characterized by X-ray diffraction (XRD), scanning electron microscopy (SEM), transmission electron microscopy (TEM), selected area electron diffraction (SAED) and X-ray photoelectron spectroscopy (XPS). The results showed that cubic Ag nanoparticles were uniformly deposited on tetragonal BiOCl nanoplates. The Ag/BiOCl heterostructures showed significantly enhanced photocatalytic performance in the degradation of methylene blue (MB) comparing with the BiOCl nanoplates. The observed degradation of MB over 10 wt% Ag/BiOCl photocatalyst was 0.011 min^{-1} which is 4.58 times of that over pure BiOCl nanoplates.

1. Introduction

Bismuth oxyhalides (BiOX: X = Br, Cl and I), belonging to the family of V–VI–VII ternary oxide materials, are recently demonstrated to be new group of promising photocatalysts and energy conversion due to their uniquely excellent electrical, magnetic, optical, luminescence and catalytic properties [1–3]. Bismuth oxychloride (BiOCl), a p-type semiconductor with its band gap of 3.5 eV, is a representative of bismuth oxyhalide and has unique properties such as high stability and relatively superior photocatalytic ability [1, 2, 4]. It shows much higher photocorrosion stability than BiOBr and BiOI [2]. BiOCl is a layered structure consisting of highly anisotropic layered structure with stacking of $[Bi_2O_2]^{2+}$ layers along the z axis with the accessibility of ultrathin BiOCl nanosheets with largely exposed (001) plane [1, 2, 5]. Thus, the transfer process of photogenerated carriers inside the crystal can be accomplished with very smooth, leading to prolong the lifetime of photoinduced carriers [2]. To develop the photocatalytic efficiency, the separation of photo-induced electron–hole pairs is improved by reducing the recombination rate of electron and hole in BiOCl and is crucial for photocatalytic efficiency [6]. In

---

general, formation of heterojunction by depositing a noble metal such as Pd, Au and Ag [7–12] is to prevent recombination of photo-induced electrons and holes and to improve the photocatalytic activity [7]. Ren et al. [7] succeeded in preparing of Pd/BiOCl/BiOI photocatalyst with different contents of Pd by ultraviolet radiation reduction. The results showed that 3% Pd/BiOCl/BiOI photocatalyst exhibited good photocatalytic activity. Zhu et al. [12] succeeded in the synthesis of $ZnWO_4$/Ag yolk-shell microspheres for degrading of methylene blue (MB) under xenon light irradiation. In comparison with pure $ZnWO_4$ yolk-shell microspheres, $ZnWO_4$/Ag yolk–shell microspheres displayed very good visible-light-driven photocatalytic performance through the dye photo-removal reaction.

In this research, a simple, low cost and template-free method was used to synthesize Ag/BiOCl nanocomposites by sonochemical deposition method. The nanocomposites displayed highly photocatalytic activity for the degradation of methylene blue (MB) under visible light.

2. Experiment

In a typical hydrothermal synthesis, each of $Bi(NO_3)_3 \cdot 5H_2O$ and NaCl was dissolved in 100 ml deionized water, stirred for 30 min and mixed together. Then 25 ml of 3 M NaOH was added to the mixed solution. The suspension was transferred to a 200 ml Teflon-lined autoclave and heated at 180 ^oC for 20 h. The as-synthesized precipitates were filtered, thoroughly washed and dried for further proceedings.

To prepare Ag/BiOCl nanocomposites, different weight contents (1–10 wt%) of $AgNO_3$ were dissolved in 2.5 g BiOCl suspension containing in 100 ml ethylene glycol and vibrated by ultrasonic radiation for 30 min. The as-prepared precipitates were collected, washed with deionized water three times and dried at 80 ^oC for 24 h for further characterization by X-ray diffraction (XRD), field emission scanning electron microscopy (FE-SEM), transmission electron microscopy (TEM), selected area electron diffraction (SAED) and X-ray photoelectron spectroscopy (XPS).

Photocatalytic activity was evaluated through the degradation of methylene blue (MB) as model dye solution. 0.2 g photocatalyst was added to 1×10^{-5} M of 200 ml MB solution which was magnetically stirred to form homogeneous solution. For every 30 min specific time interval, a solution was withdrawn and centrifuged. The concentration of MB was measured by a UV–visible spectrophotometer at λ_{max} of 664 nm. The degradation of MB was calculated using the below equation.

$$\text{Decolorization efficiency (\%)} = \frac{C_o - C_t}{C_o} \times 100 \qquad (1)$$

, where C_o is the initial concentration of MB and C_t is the concentration of MB after UV light irradiation within a period time (t).

3. Results and discussion

Fig. 1 shows the XRD patterns of 0–10 wt% Ag/BiOCl heterojunctions. The XRD pattern of BiOCl without Ag loading shows diffraction peaks at 2θ = 11.711°, 24.132°, 25.931°, 32.561°, 33.431°, 34.863°, 36.575°, 40.961°, 46.881°, 49.611°, 54.291°, 55.165° and 58.731° which can indexed to the (001), (002), (101), (110), (102), (111), (003), (112), (200), (113), (211), (104) and (212) planes of the tetragonal BiOCl phase (JCPDS card no. 06-0249) [13]. The results certified that pure BiOCl was successfully synthesized by hydrothermal method. No other impurity peaks were detected, indicating the synthesis of high purified BiOCl sample.
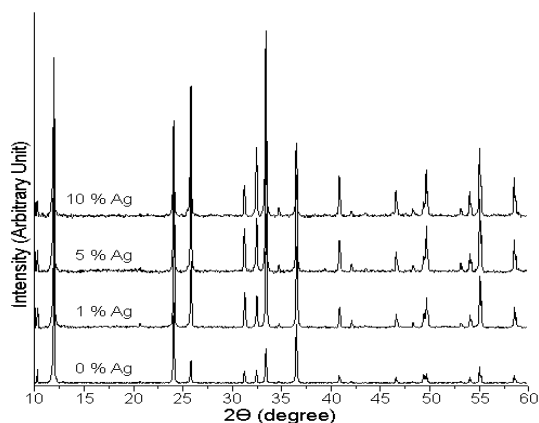
Fig. 1. XRD patterns of 0–10 wt% Ag/BiOCl nanocomposites.

It can be seen that the diffraction peak intensities of the {001} facet family such as (001), (002) and (003) become strengthened, indicating that BiOCl nanoplates should be favor to grow along the *c*-axis or [001] orientation [5]. BiOCl crystal has layered structure consisting of Bi_2O_2 slabs which are interleaved by double slabs of Cl atoms. The dominating facets of BiOCl crystal are (001) and (110) [1, 2]. For the 1 wt%, 5 wt% and 10 wt% Ag/BiOCl samples, the XRD patterns of Ag/BiOCl heterojunctions with different weight contents of Ag containing in BiOCl show main diffraction peaks of tetragonal BiOCl phase. Nevertheless, cubic Ag phase was not detected in these XRD patterns because the content of Ag is very low and particle size of Ag containing in Ag/BiOCl heterojunctions is very low [14–16]. In addition, no distinct peak shift was detected in XRD spectra of Ag/BiOCl heterojunctions, implying that Ag nanoparticles attached on the surface of BiOCl.
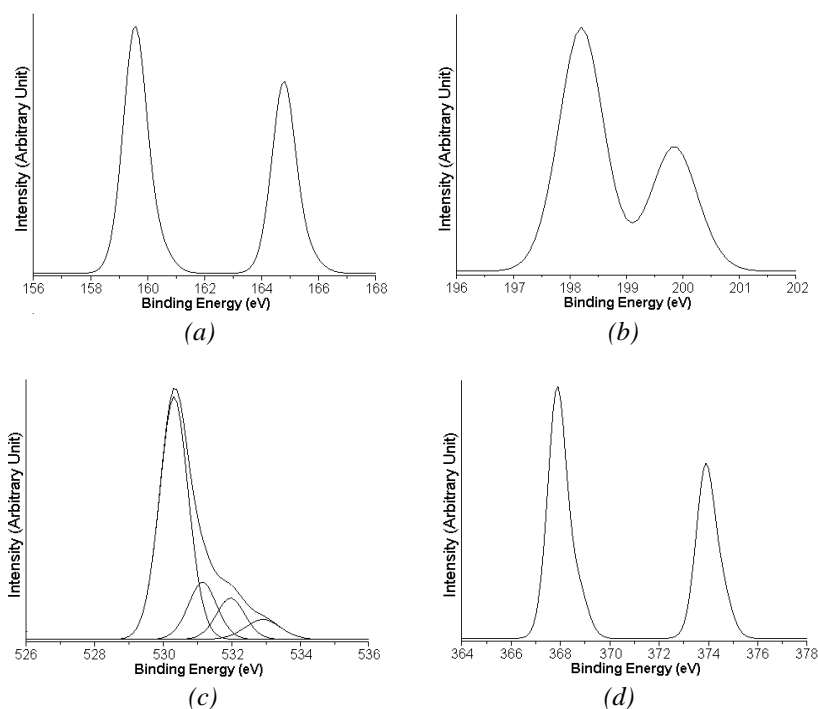

Fig. 2. XPS spectra of (a) Bi, (b) Cl, (c) O and (d) Ag atoms of 10 wt% Ag/BiOCl photocatalyst.

XPS analysis was used to further investigate the surface components and bond states of the as-prepared Ag/BiOCl heterostructure. Fig. 2 shows the XPS spectra of Bi, Cl, O and Ag elements containing in Ag/BiOCl heterostructure. Fig. 2a shows the binding energy peaks at 159.40 eV and 164.67 eV which are assigned to Bi $4f_{7/2}$ and Bi $4f_{5/2}$ of BiOCl lattice [2, 3, 4, 6]. They certify that the main chemical species of bismuth is Bi^{3+} [6, 7]. The binding energies of Cl $2p_{3/2}$ and Cl $2p_{1/2}$ were detected at 198.11 eV and 199.70 eV (Fig. 2b) which are in consistent with the binding energies for Cl^- of BiOCl lattice [2, 3, 4, 6]. The O 1s spectrum as shown in Fig. 2c can be de-convoluted into four peaks at 530.11 eV, 531.19 eV, 532.01 eV and 532.87 eV. The binding energies of O 1s are contributed to the lattice oxygen of Bi–O bond (530.11 eV) and Br–O bond (531.19 eV) of BiOCl lattice [2, 3, 4]. Other binding energies of O 1s peaks are in accordance with contaminated carbon (C–O) and oxygen of adsorbed water on surface of the material [2, 14, 15]. The binding energies of Ag 3d core level (Fig. 2d) of Ag $3d_{5/2}$ (367.85 eV) and $3d_{3/2}$ (373.87 eV) were detected in 10 wt% Ag/BiOCl sample [16, 17]. The energy space of 6.02 eV between these two corresponds to the characteristic peak of metallic silver [15], indicating the existence of silver nanoparticles. Clearly, metallic silver nanoparticles were supported on the surface of BiOCl.

The morphology and crystallographic growth direction of the BiOCl and 10 wt% Ag/BiOCl samples were investigated by SEM, TEM and SAED techniques as the results shown in Fig. 3. SEM and TEM images of the pure BiOCl sample show that product formed from uniform BiOCl nanoplates with edge length of 2–3 µm and thickness of 200–300 nm. SAED pattern of a single BiOCl nanoplate was studied for the perspective of crystalline facets of BiOCl nanoplate. It appears as spot pattern which indicated a single crystal. The calculated diffraction spots correspond to the (1–10), (200) and (110) planes with the [001] direction as zone axis. Based on the results and the symmetry of tetragonal BiOCl, the bottom and top surfaces of the BiOCl nanoplate can be identified as {001} facets and the edge surfaces as {110} facets [6, 18, 19]. Comparing with pure BiOCl, the morphology of Ag/BiOCl heterostructure with Ag content of 10 wt% remains unchanged. Ag nanoparticles were detected on the surface of BiOCl nanoplates, implying that Ag nanoparticles prepared by the reduction reaction of $AgNO_3$ by sonochemical method.

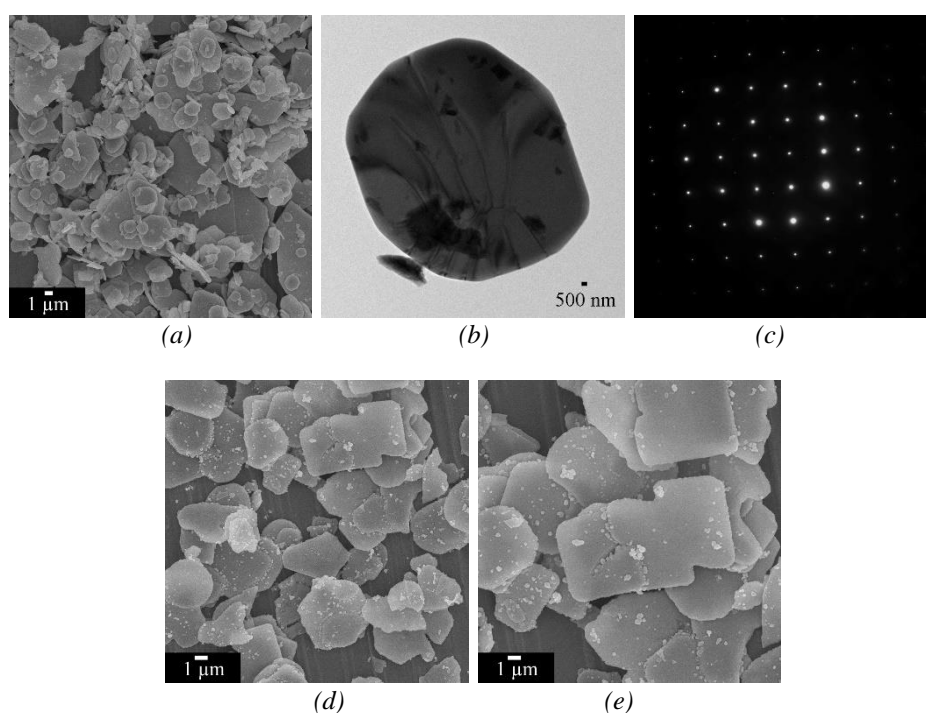*(a)*   *(b)*   *(c)*

(d)   *(e)*

Fig. 3. SEM and TEM images, and SAED pattern of (a–c) BiOCl and (d, e) 10 wt% Ag/BiOCl nanoplates.

The photocatalytic performance of 0–10 wt% Ag/BiOCl nanoplates were evaluated by photocatalytic degradation of MB solution under UV light irradiation within 300 min as the results shown in Fig. 4a. It can be seen that pure MB solution in the absence of photocatalyst is rarely degraded under the visible light. The photocatalytic efficiency of BiOCl nanoplates is greatly enhanced as the weight content of Ag increases. The BiOCl nanoplates photodegraded only 51.26 % of MB and the 10 wt% Ag/BiOCl heterostructure photodegraded 97.57 % of MB within 300 min. The 10 wt% Ag/BiOCl heterostructure presents the photocatalytic efficiency 1.90 times of the pure BiOCl nanoplates.

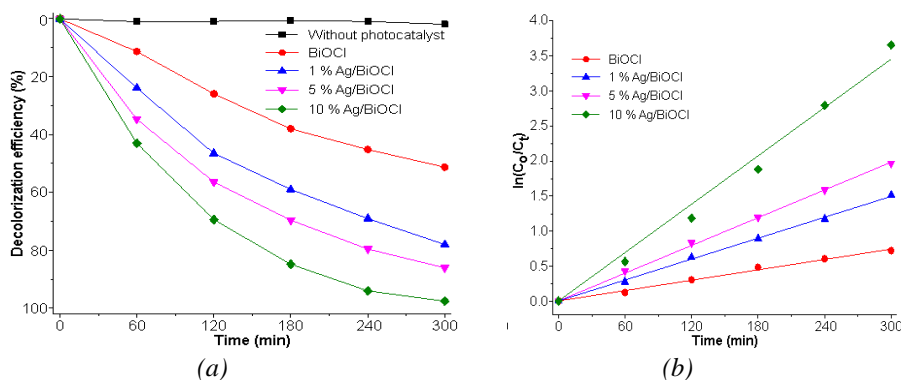*(a)*   *(b)*

Fig. 4. (a) Decolorization efficiency and (b) first-order plot for photocatalytic degradation of MB by 0–10 wt% Ag/BiOCl nanoplates under UV light irradiation with respect to that of MB solution without photocatalyst.

In this research, the photocatalytic degradation of MB obeyed the pseudo-first-order kinetics of the Langmuir–Hinshelwood model related to the adsorption of heterogeneous photocatalyst [5, 14, 15]. The photocatalytic degradation is expressed as

$$-\ln(C_t/C_0) = kt \qquad (2)$$

, where t, k, C_t and C_0 are the degradation time, the apparent first-order rate constant, the MB concentration at t = t and t = 0, respectively. Fig. 4b shows the reaction kinetics profile of BiOCl and Ag/BiOCl heterostructures. All reactions obey the pseudo-first-order kinetics of which the slopes are the reaction kinetics [14–16]. The k values for photodegration of MB are 2.4 x 10^{-3}, 4.9 x 10^{-3}, 6.5 x 10^{-3} and 0.011 min^{-1} for BiOCl, 1 wt% Ag/BiOCl, 5 wt% Ag/BiOCl and 10 wt% Ag/BiOCl, respectively. The k value increases remarkably with increasing in the weight content of Ag loaded on BiOCl photocatalyst. The k value for 10 wt% Ag/BiOCl is 4.58 times of that for BiOCl.
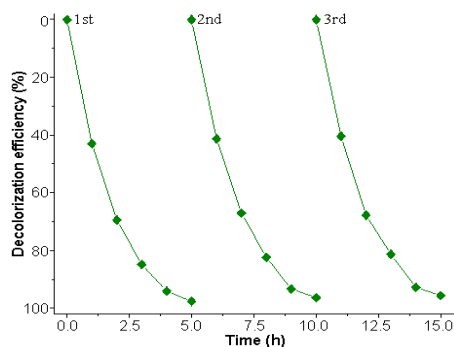

Fig. 5. Recyclability for photocatalytic degradation of MB by 10 wt% Ag/BiOCl nanoplates.

In this research, the stability of 10 wt% Ag/BiOCl was also investigated. After photocatalytic reaction, the suspension was centrifuged, filtered, washed several times with distilled water and dried at 110 °C in an electric oven. At the end of the third cycle (Fig. 5), the reused 10 wt% Ag/BiOCl nanoplates showed very high photocatalytic stability.
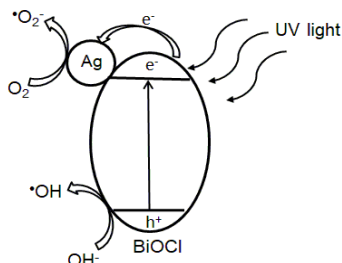

Fig. 6. Schematic diagram for separation of electron-hole pairs between Ag and BiOCl photocatalyst.

Fig. 6 shows a mechanism for photocatalysis of Ag/BiOCl nanoplates. The photoexcited electrons and photogenerated holes were created in conduction and valence bands of BiOCl induced by UV light irradiation. The photogenerated electrons in conduction band of BiOCl diffused to Ag nanoparticle. The electrons were trapped by adsorbed O_2 to produce $^\bullet O_2^-$ radical. Concurrently, the photogenerated holes in valence band of BiOCl reacted with adsorbed OH^-/H_2O to form $^\bullet OH$ radical. Then, $^\bullet O_2^-$ and $^\bullet OH$ radicals attacked the MB molecules which were degraded and transformed into H_2O and CO_2 as final products [20]. Consequently, the recombination of photogenerated carriers was effectively suppressed. The results led to increase photocatalytic efficiency by being loaded with Ag nanoparticles on BiOCl nanoplates.

4. Conclusions

Ag/BiOCl nanocomposites were fabricated by hydrothermal method combined with sonochemical method. The Ag/BiOCl heterostructures show good deposition of Ag nanoparticles on the surface/interface of BiOCl nanoplates. The Ag/BiOCl heterostructures played the role in enhancing the separation efficiency of photogenerated electron-hole pairs which exhibited much improvement of photocatalytic activity and reusability for photodegradation of MB solution under UV light irradiation.

Acknowledgement

References

[1] H. Li, L. Zhang, Curr. Opin. Green Sust. Chem. **6**, 48 (2017).
[2] X. Ma, Z. Ma, T. Liao, X. Liu, Y. Zhang, L. L. Li, W. Li, B. Hou, J. Alloy. Compd. **702**, 68 (2017).
[3] C. Yang, F. Li, M. Zhang, T. Li, W. Cao, J. Molecular Catal. A **423**, 1 (2016).
[4] S. Zhu, C. Yang, F. Li, T. Li, M. Zhang, W. Cao, Molecular Catal. **435**, 33 (2017).
[5] B. Li, L. Shao, B. Zhang, R. Wang, M. Zhu, X. Gu, J. Colloid Interf. Sci. **505**, 653 (2017).
[6] D. Chen, M. Zhang, Q. Lu, J. Chen, B. Liu, Z. Wang, J. Alloy. Compd. **646**, 647 (2015).
[7] L. Z. Ren, D. E. Zhang, X. Y. Hao, X. Xiao, Y. X. Jiang, J. Y. Gong, F. Zhang, X. Zhang,

Z. W. Tong, Mater. Res. Bull. **94**, 183 (2017).

[8] L. Ge, Mater. Lett. **62**, 926 (2008).

[9] X. Liu, Y. Kang, D. Luo, Mater. Lett. **185**, 189 (2016).

[10] C. Yu, Y. Yu, T. Xu, X. Wang, M. Ahmad, H. Sun, Mater. Lett. **190**, 185 (2017).

[11] S. Li, Y. Zhao, C. Wang, D. Li, K. Gao, Mater. Lett. **170**, 122 (2016).

[12] J. Zhu, M. Liu, Y. Tang, T. Sun, J. Ding, L. Han, M. Wang, Mater. Lett. **190**, 60 (2017).

[13] Powder Diffraction File, JCPDS-ICDD, 12 Campus Bld, Newtown Sq, PA 19073-3273, USA, 2001.

[14] A. Phuruangrat, P. Dumrongrojthanath, S. Thongtem, T. Thongtem, Mater. Lett. **194**, 114 (2017).

[15] A. Phuruangrat, P. Dumrongrojthanath, B. Kuntalue, S. Thongtem, T. Thongtem, Mater. Lett. **196**, 256 (2017).

[16] A. Phuruangrat, S. Putdum, P. Dumrongrojthanath, N. Ekthammathat, S. Thongtem, T. Thongtem, Mater. Sci. Semicond. Process. **34**, 175 (2015).

[17] A. Phuruangrat, A. Maneechote, P. Dumrongrojthanath, N. Ekthammathat, S. Thongtem, T. Thongtem, Mater. Lett. **159**, 289 (2015).

[18] K. Li, Y. Liang, J. Yang, Q. Gao, Y. Zhu, S. Liu, R. Xu, X. Wu, J. Alloy. Compd. **695**, 238 (2017).

[19] X. Hu, Y. Xu, H. Zhu, F. Hu, S. Zhu, Mater. Sci. Semicond. Process. **41**, 12 (2016).

[20] Y. L. Qi, Y. F. Zheng, X. C. Song, J. Alloy. Compd. **726**, 1147 (2017).